INTERNATIONAL JOURNAL OF
ENERGY AND ENVIRONMENT

Volume 5, Issue 3, 2014 pp.275-296
Journal homepage: www.IJEE.IEEFoundation.org

A numerical investigation of flow profile and performance of a low cost Crossflow turbine

Chiyembekezo S. Kaunda[1], Cuthbert Z. Kimambo[2], Torbjorn K. Nielsen[1]

[1] Waterpower Laboratory, Department of Energy and Process Engineering, Norwegian University of Science and Technology, Trondheim 7491, Norway.
[2] Department of Mechanical and Industrial Engineering, University of Dar es Salaam, P.O. Box 35091, Dar es Salaam, Tanzania.

Abstract
Low efficiency is the main drawback of a Crossflow turbine, despite the turbine being an important low cost technology for micro hydropower generation. Poor flow profile has been mentioned by other Crossflow turbine performance investigators as one of the reasons for the underperformance. This paper has investigated, using numerical method, the flow profile in the turbine at best efficiency point and at operating conditions that are away from best efficiency point. Numerical method has also been used to calculate and predict the efficiency of the turbine.
The flow physics in a Crossflow turbine runner is a two-phase with a movable free surface. Such flow physics is difficult to analyse even numerically. A procedure for numerical analysis was followed and ANSYS CFX® was used to solve the governing equations and to process the simulation results. Actual pictures of the flow were taken so as to compare the actual flow with the numerically determined flow profile. Turbine efficiency results from the previous performance evaluation experiment conducted on the model Crossflow turbine were compared with the numerically obtained efficiency results. It has been observed that the numerically obtained flow profile compare favorably with the actual flow pictures. The numerical analysis over-predicts the efficiency, especially for runner speeds that were more than the best efficiency point speed.
Pockets of negative pressures and flow circulation have been observed in the flow profile. At constant head and valve opening, the velocity profile was found to vary more with runner speed than the pressure profile. The numerically obtained flow pattern showed positions where the flow gives maximum efficiency. Therefore, the study has shown that numerical method is a superior design tool for Crossflow turbines.

Keywords: Micro hydropower; Crossflow turbine; Turbine performance, Numerical analysis; Flow analysis.

1. Introduction

1.1 General background

Microhydropower is an important renewable energy source especially in countries that have perennial rivers and topographies that are mountainous. Currently, most of the installed microhydropower (MHP) plants are used to generate electricity. If the turbine shaft is extended from both sides, mechanical power

can also be generated together with electrical power. The sizes of MHP plants defined in terms of installed electrical capacity are numerous but with no international consensus. However, the definition of 'up to 100 kW installed capacity' seems to be common amongst countries and international development organisations. On the basis of off-grid rural power supply, such a capacity is robust enough to provide power to support domestic and some small-scale business applications. The MHP systems, therefore, are useful in supporting social and economic development activities in rural communities.

Crossflow turbine (CFT) is arguably the simplest turbine to design and manufacture. For this reason, they are among the low cost MHP technologies. They are widely used for rural power supply in some countries of Asia such as Nepal. International charitable organisations such as Practical Action (formerly called Intermediate Technology Group), Swiss Centre for Appropriate Technology (SKAT) and German Technical Operation Agency (GTZ) have been very pivotal in the development of the CFT technology in developing countries. These organisations, like SKAT, were interested in the development of a very low cost CFT, thereby modifying some basic parts of the original Crossflow turbine as designed by Prof. Banki. Therefore, it can be said that the CFT technology has been promoted basically as 'an appropriate technology' and not necessarily as a special 'industry-made' turbine.

The CFT can be applied in a wide range of flow and head. However, it has a general drawback of inferior performance compared to other turbines used in MHP applications. This has contributed to the turbine not being promoted by turbine manufacturers in the same way as Francis, Pelton and Kaplan turbines. The original CFT turbine, as proposed by Prof. Banki, had a maximum theoretical efficiency of 87.8% [1]. However, upon building and testing the turbine, Mockmore and Merryfield in 1949 obtained an efficiency of 68% [1]. This indicated the need for CFT performance improvement. Consequently, the CFT has been subjected to several performance improvement studies (such as those in Table 1).

Table 1. Some Crossflow experimental studies and maximum efficiency levels attained

Investigators	Maximum efficiency (%)
Mockmore and Merryfield [1]	68
Nakase *et. al.* [2]	82
Johnson *et. al.* [3]	80
Durgin and Fay [4]	66
Khosrowpanah [5]	80
Hothersall [6]	75
Ott and Chappel [7]	79
Desai and Aziz [8]	88
Olgun [9]	72
Andrade *et. al.* [10]	78

Most of the CFT performance improvement studies have concentrated on optimising its geometric design parameters (such as number of blades, runner diameter, width, nozzle and nozzle entry arc) using laboratory based experiments. As it can be seen from Table 1, different investigators have reported diverse values of maximum efficiencies. Despite the fact that these results may have depended on the laboratory settings and other controls of design parameters, the results still indicate room for further performance improvement.

The other room for performance improvement is in the area of improving turbine flow profile [10]. Poor flow profile is associated with efficiency reduction. Flow profile can be known from flow characterisation. Flow in the turbine can be characterised by solving the Navier-Stokes equations in the flow domain using analytical and numerical methods. Analytical solution, which gives a continuous solution to the Navier-Stokes equations, is nearly impossible due to non-linearity of the equations and the complexity of the turbine flow. An alternative is the numerical analysis, which gives discrete solution to the equations.

Experimental methods are also used in analysing flow profile in the rotating runner. These methods include visualising the flow by photographing using high speed camera. Sometimes a stroboscope is used to 'bring the flow to a halt or very low speed' and the flow pattern can then be visualised and photographed. The visibility in the flow visualisation experiments can be enhanced by injecting a dye in the flow. Pitot tubes can be used to characterise the flow velocity profile, from which, using the Bernoulli's equation, pressure profile can be determined. Experimental methods have the advantage that

they can capture the exact flow profile and are therefore, also used to validate analytical and numerical flow characterisation results.
Experimental, as with analytical methods, have limitations in charactering flow with complex flow geometries as in CFT. Currently, numerical analysis is becoming an important industrial tool in characterising the flow during the turbine design process. With advancements in computational fluid dynamic (CFD) solvers and tools for post-processing of the numerical results, the capacity of numerical method in the design of complex turbines has been enhanced.
The determination of flow field in terms of pressure and velocity fields is important in the design of a high performance turbine because regions of poor flow (for example, regions of flow recirculation and negative pressure) can be identified. Once regions of poor flow profile are identified, the turbine performance can be improved through optimization of geometric and dynamic design parameters.

1.2 Numerical method overview
In general, a numerical analysis procedure involves the following steps: i) development of governing equations for the flow physics; ii) discretising the equations in both time and space, iii) discretising the flow domain (meshing); iv) solving the discretised equations using a computerised solver (or program) and v) post-processing of the results using a computerised program. It is necessary to validate the numerical results by comparing them with experimental results.
As stated already, numerical analysis is currently the standard way of designing turbines in the industry. Numerical analysis for predicting the performance of impulse turbine runners poses a special challenge because of complexity of the flow physics. In impulse turbines like CFT, the jet flow in the runner is intermittent and there is a movable free surface boundary between the jet and surrounding air. This means that the actual flow is unsteady and two phase with a movable free surface. Two approaches are being used to numerically analyse such a flow. These approaches are particle tracking method and a classical CFD method where a free surface is tracked.
The particle tracking method does not require discretisation of the flow domain; it uses Lagrange principle of following the path of a fluid particle. This method has been used by various turbine designers to design Pelton turbine runners, for example Zoppe *et. al.* in 2006 [11]. The classical CFD method where a free surface is tracked is generally referred to as volume-of-fluid method. In terms of computational costs, the classical CFD is superior to particle tracking method. This study employs a classical CFD method.
Some previous investigators have attempted to numerically study the flow through the nozzle and the runner of CFTs. Fukutomi *et. al.* in 1991 and 1995 [12, 13] numerically characterized the flow in the CFT runner and calculated unsteady forces acting on the blades, assuming only water in the turbine. Pereira and Borges in 1996) [14] used two-dimensional CFD to simulate the flow inside the CFT nozzle. Arzola *et. al.* in 2008 [15] conducted three-dimensional free surface CFD simulations inside the nozzle where influence of angles of attack on performance was investigated. Choi *et. al.* in 2008 [16] employed water-air free surface CFD simulations to investigate effect of varying nozzle shape, blade angle and number of blades on performance.

2. Crossflow turbine technology

2.1 Crossflow turbine history
Crossflow turbine is first reported to be invented by an Australian Engineer, Anthony Mitchell, who patented the original design in 1903 [17]. It is also reported that a Hungarian mechanical engineer, Professor Donat Banki, refined it through series of experiments between 1916 and 1918 in West Germany [17]. JLA & Co. Limited in 2010 states that by 1920, the turbine was well known in Europe [18]; may be as a result of Banki's research publications. It is further reported that a German engineer, Fritz Ossberger, collaborated with Mitchell and worked on the development of the turbine. In 1933, Ossberger obtained the German Imperial patent for the turbine [19]. Therefore, it is convenient to state that Mitchell, Banki and Ossberger played important roles in developing the Crossflow turbine technology. This explains why the Crossflow turbine is also known as Banki or Mitchell or Ossberger turbine or their combinations.
The original CFT design was developed based on impulse principle [1]. A gap was left between the nozzle and the runner, as shown in Figure 1(a), so that the jet from the nozzle entered the runner at an atmospheric pressure. Recent modifications in the design have removed the gap between the nozzle and

the runner resulting in the nozzle following the runner closely, as shown in Figure 1(b). This causes the jet entering the turbine to have a positive pressure [20, 21].

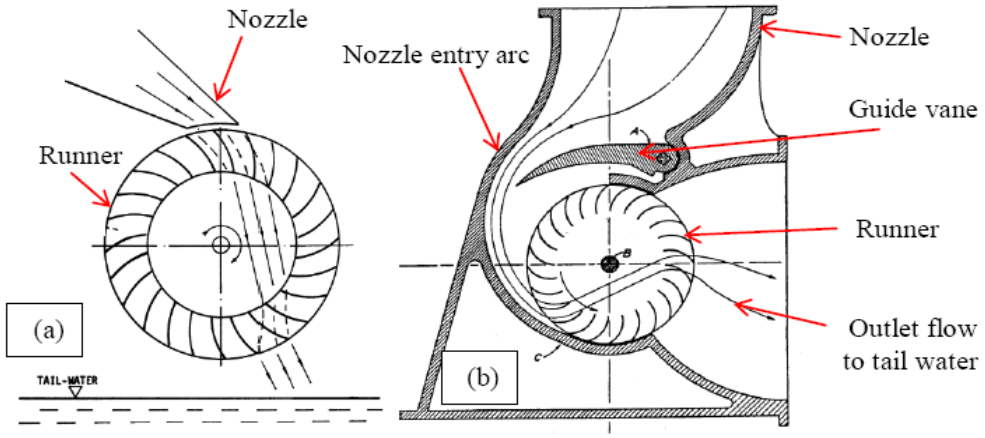

Figure 1. (a) Pure impulse Crossflow turbine where a gap is left between the runner and nozzle; (b) Modified Crossflow turbine where the nozzle wall follow the runner closely [1]

2.2 Crossflow turbine physical description

Crossflow turbine is basically composed of runner and nozzle (Figure 1). For low cost projects, the runner is simply a fabricated squirrel-cage-shaped device that is made of two or more circular discs joined together by curved horizontal blades. The runner blades can be cut from a standard sheet metal or steel pipe and then be bent into the required blade profile. In some cases, to improve on the structural integrity of the runner, more than two equally spaced discs are employed. The discs are then keyed into the shaft which is supported by two bearing housing.

The CFT nozzle is traditionally a convergent pipe with rectangular cross-section at inlet and outlet. It has four walls: two are parallel fixed plane walls and the other two walls can be made of cylindrical or spiral logarithmic shapes. The nozzle, apart from converting pressure energy into kinetic energy in form of water jet, also directs and regulates flow (jet) into the runner using a guide vane. The nozzle can be fabricated from the sheet metal and other materials. For example, Durgin and Fay in 1984 [4] used relatively cheap Plexiglas for nozzle walls.

To simplify the design, some versions of the CFT nozzles do not have guide vanes. Instead, the flow is controlled by one of the curved wall of the nozzle that is made movable. To simplify the design further, the movable wall can be a simple 'flap' which is operated by a screw (Figure 2). In this project, the last version of the nozzle is used.

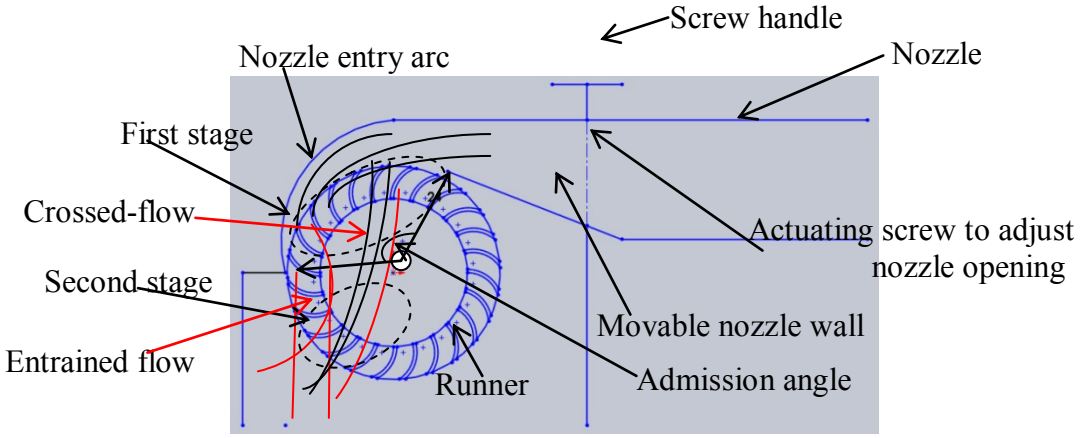

Figure 2. Schematic diagram of a low-cost Crossflow turbine used in this project and some basic flow terminology

The nozzle can be oriented in vertical, horizontal or slanting positions. For relatively high cost company-manufactured CFT, the runner can be partitioned so that the jet, through the nozzle, is channelled to the

specific portion depending on flow availability (and sometimes on power requirement). Technically, these are the most versatile and efficient Crossflow turbines, but the requirement of the nozzle with more than one guidevanes to guide the portion of water is an extra cost. This extra cost cannot be justified for low cost MHP systems.

2.3 Flow description in the Crossflow turbine runner

The jet flow in the CFT runner can be described in the following manner. The jet issued from the nozzle is directed to the runner. The jet then exchanges energy with the runner in two distinct stages (Figure 2). Firstly, the water jet flows through the runner blades from the periphery towards the centre. This is the first stage. Then, after crossing the open centre space of the runner, the jet flows from the inside of the runner towards its outer periphery, from where it is discharged to the tailrace water. This is the second stage. This flow phenomenon has made CFT to be regarded as a two-stage partial 'impulse' turbine. Due to partial flow in the runner blades and flow in the open centre space, the jet flow inside of the runner is essentially two phase, namely water and air.

The first stage may operate with a degree of reaction. The second stage operates on pure impulse principle because the jet exits first stage and enters second stage at an atmospheric pressure due to presence of open space between stages. The flow within the runner blade can be modelled as radial flow. Because of this, there is a possibility for the jet to strike the shaft in the open space, thereby increasing losses and spoiling flow incident angles to the second stage.

Not all of the flow from the nozzle crosses the runner. The flow that crosses the runner blades is known as the crossed-flow. Some of the flow from the nozzle is entrained within the blades. The remaining flow gets leaked through the clearance between the runner periphery and the turbine housing. It is only the crossed-flow that takes part in energy transfer to the runner blades. Therefore entrained and leakage flows both reduce the power output of the turbine.

The flow can be entrained if it is decelerated in the radial direction by back pressure or centrifugal forces of the flow. The entrained flow is flushed out tangentially from the runner. The entrained flow analysis is an area that has not been studied extensively. The CFT theory from Prof. Banki CFT design did not even include it. The published experimental results of Durgin and Fay in 1984 [4] provide some information that the entrained flow depends on flow angle, flow velocity, runner velocity, runner geometry and nozzle geometry.

The leakage flow can be limited to smallest practically possible amount. Complete elimination is not possible because clearance is required between rotating runner and housing. The leakage flow also depends on the flow pressure, especially if the turbine operates more on reaction mode than on impulse mode.

3. Research objectives

The main objective of this study is to numerically characterize the two-phase flow in the Crossflow turbine. Specifically, the study will:

a) At constant head, determine using computational fluid dynamic approach the flow pressure and velocity fields in the turbine both at best efficiency and outside the best efficiency conditions.
b) Analyze the effect of flow pattern on efficiency and compare with experimentally obtained efficiency values.

The goal of this study is to achieve a better use of microhydropower resources with efficient low-cost Crossflow turbine designs.

4. Model Crossflow turbine description

The dimensions of the Crossflow turbine used in this study are those of the actual simplified Crossflow turbine that was tested at Waterpower Laboratory at the Norwegian University of Science and Technology in 2013. The performance test established the best efficiency point and the general performance of the turbine with varied head, flow and runner speed from the best efficiency point. The experimental results are used to validate the numerical results on performance assessment. The best operating point of 79% was identified at 5m head, 350 rpm and a nozzle opening of 80%.

As already stated, the simplified CFT used in this study does not have a guide vane. The flow in the nozzle is controlled by a flap that is operated via a screw handle (Figures 3 and 4). Figure 3 shows the schematic drawing of the simplified CFT. The normalized design parameters are given in Table 2.

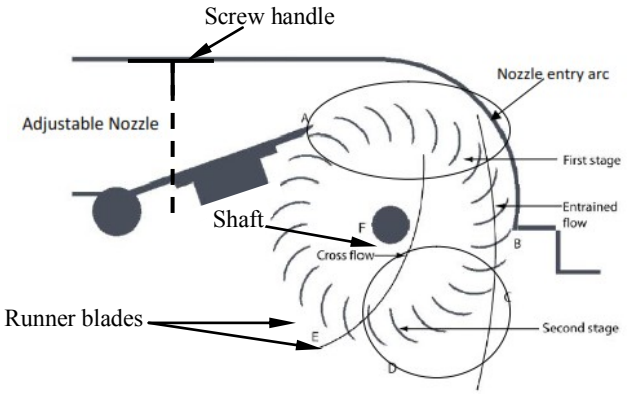

Figure 3. Schematic sketch of the model Crossflow turbine

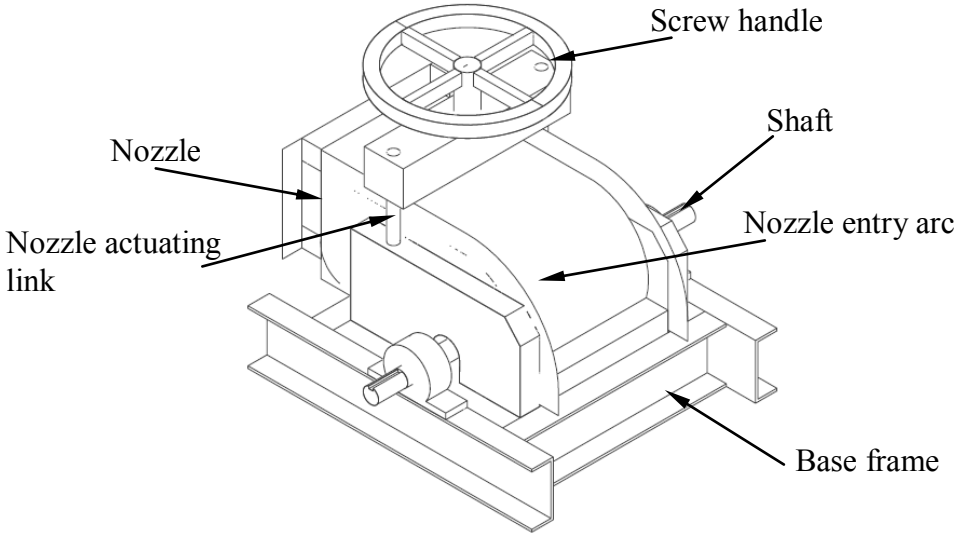

Figure 4. Pictorial sketch of the model Crossflow turbine housing

Table 2. Details of the Crossflow turbine design parameters used in the numerical study

Design parameter	Normalized expression	Value
Diameter ratio D_1 is outside diameter of runner D_2 is the inside diameter of the runner	$\frac{D_2}{D_1}$	0.693
Angle of attack	α	16 degrees
Blade angle (outside runner periphery)	β_1	30 degrees
Blade angle (inside runner periphery)	β_2	90 degrees
Radius of the blade (r_b)	$\frac{r_b}{D_1}$	0.157
Radius from centre of the runner to the centres of where blades are drawn	$\frac{R}{D_1}$	0.378
Admission arc	φ	90 degrees
Number of blades	n_b	24
Nozzle opening	$\frac{l}{D_1}$	0.254
Nozzle width where W is the runner width	$\frac{B}{W}$	1
Radius of the nozzle entry arc	$\frac{r_{(\emptyset)}}{D_1}$	0.567

5. Methodology

The numerical analysis for this study was performed in ANSYS Workbench® 2012 where ANSYS CFX Project with its subprograms, namely: Geometry, Mesh, ANSYS CFX-Pre, ANSYS CFX solver and ANSYS Post-processing, was used. As stated already, numerical analysis require coming up with a flow domain which has to be discretised (or meshed) in space and time (for unsteady state analysis). The flow domain (Figure 5) was designed in 'Geometry' sub-program using the ANSYS Design Modeler.

The flow domain consists of the nozzle, turbine casing and the runner. The nozzle and turbine casing were designed in ANSYS Design Modeler while the runner was designed in Solidworks® 2012. In the ANSYS Design Modeler, the runner was imported and positioned at the required central position.

This numerical analysis involves the runner, which has a rotating frame of reference while the nozzle and turbine casing have non-rotating frame of reference (stationary frame of reference). The numerical problem can be solved by using the 'multiple frame of reference' as detailed in ANSYS Theory Guide of 2010 [22]. The 'multiple frame of reference' requires dividing the flow domain into flow zones with the aim of isolating the zone that has a rotating frame of reference. To ensure continuity of flow, the zones (or domains) are interfaced. In this case, three flow zones were created. The zone with rotating frame of reference is isolated, as shown in Figure 6. The other two zones are assigned names: 'turbine casing zone' and 'non-rotating zone' and are given non-rotating frame of reference.

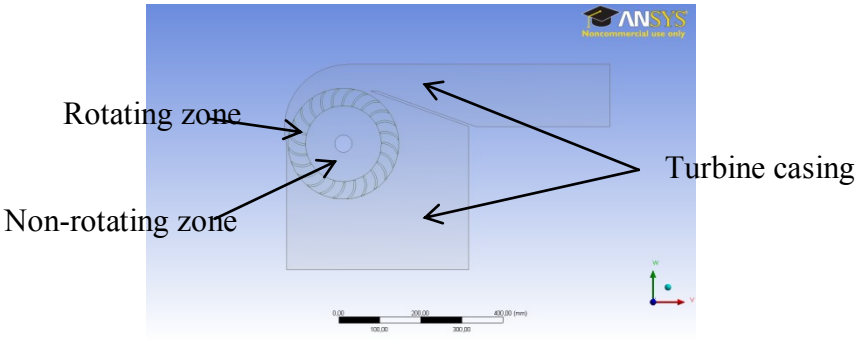

Figure 5. Crossflow turbine runner showing flow zones

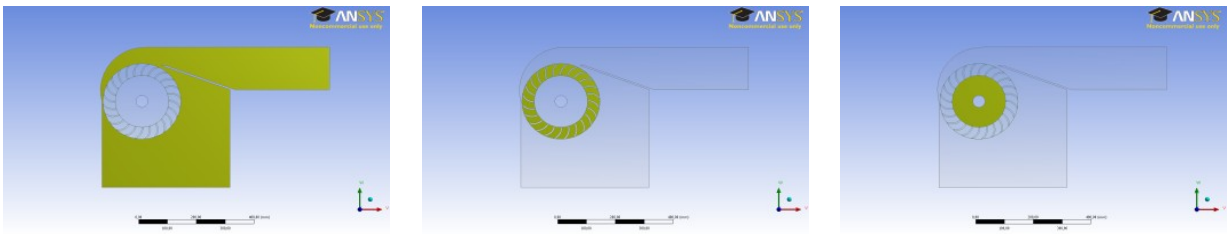

(a) (b) (c)

Figure 6. Specified flow zones by shading: (a) Turbine casing zone; (b) Rotating zone; (c) Non-rotating zone

The flow domain was meshed using the ANSYS Mesh sub-program of the ANSYS CFX Project. The mesh properties are given in Section 5.2. The mesh sensitivity analysis was performed (Section 5.3) to make sure that the solution obtained is independent of the mesh.

Modeling of the physics of the flow problem was done in the ANSYS CFX-Pre, a subprogram after meshing in the ANSYS CFX. Modeling of the flow physics included creating interfaces for flow zones (or domains), assigning boundary conditions, assigning initial conditions, applying governing equations with appropriate turbulence models and choosing the flow materials (water and air) and their phase properties. The solution control and declaration of variables were also done in the ANSYS CFX-Pre.

The domains were interfaced using the general connection model in the ANSYS CFX-Pre. The meshes in the domains were connected using the general grid interface model. Frozen rotor principle was used to model frame mixing process for the rotating and non-rotating frames of flow domains at the interfaces. In the frozen rotor model, the frame of reference and/or pitch is changed but relative orientations of the components across the interface remain fixed. In this way, the relative positions of components during calculations remain fixed.

The frozen rotor model produces a steady state solution to the multiple frame of reference problems, with some account of the interaction between the two frames but falls short of modelling the transient effects in the vicinity of the interface. The ANSYS CFX performs appropriate equation transformations when the frame of reference changes. The frozen rotor model requires least amount of computational cost compared to other frame mixing models that are available in ANSYS CFX. Frozen rotor model is recommended in frame mixing situations where the circumferential variation of the flow is large relative to the component pitch and where the flow domain has a rotating element [22].
The boundary conditions were prescribed at inlet, outlet, wall and interface locations of the turbine, as shown in Table 3.

Table 3. Details of the boundary conditions for the ANSYS CFX simulations

Location (s)	Assigned boundary condition type	Boundary condition details
Inlet	Inlet	• static pressure according the operational head for the particular simulation • volume fraction of 1 for water and 0 for air
Outlet	Opening	• atmospheric pressure • volume fraction of 0 for water and 1 for air
runner, nozzle and casing walls	Wall	• all walls were assigned 'non-slip' condition • wall boundary condition default details
Non-rotating zone and rotating zone interface	Interface	• Frozen rotor frame mixing model • Interface boundary condition default details
Turbine casing zone and rotating zone interface	Interface	• Frozen rotor frame mixing model • Interface boundary condition default details

A standard homogenous free surface model was used when modeling two-phase flow in the turbine runner. In the standard homogenous free surface model, both fluids (air and water) are assumed to share the same velocity, pressure and turbulence fields. Flow properties for air and water necessary for simulation were obtained from the ANSYS Library. Salient parameters for two-phase simulation are given in Table 4 in 'Fluid pairs'.
A second order upwind discretisation scheme was used for the governing equations. Viscous fluxes were computed with a high resolution scheme. To ensure computational robustness, locations where gradient changed abruptly, a first-order upwind scheme was applied. The rest of solver controls and salient simulation parameters are given in Table 4.

5.1 Governing equations
The equations used in this numerical flow analysis are the Reynolds Averaged Navier Stokes (RANS) equation with turbulence models based on eddy viscosity concept. As already stated, this is a two-phase flow problem with a movable free surface and that one of the flow domain has a rotating frame of reference. In this case, the effective density of each phase is given in terms of its volume fraction. For the rotating zone, the RANS for the momentum equations are modified to take into account centrifugal and Coriolis forces, as detailed in ANSYS Theory Guide [22]. These forces cannot be ignored in a rotating frame of reference. The modified RANS equations are given in equations (1) and (2). The Table 5 lists the meaning of the symbols used in the modified RANS equations and the modified pressure equation (3).

$$\frac{\partial(\alpha_p \rho_p)}{\partial t} + \nabla \cdot \left(\alpha_p \rho_p \vec{V}_r\right) = S_p \tag{1}$$

$$\frac{\partial\left(\alpha_p \rho_p \vec{V}_r\right)}{\partial t} + \nabla \cdot \left(\alpha_p \rho_p \vec{V}_r \otimes \vec{V}_r\right) - \nabla \cdot \left(\mu_{eff} \nabla \vec{V}_r\right) + \alpha_p \rho_p (2\vec{\omega} \times \vec{V}_r + \vec{\omega} \times \vec{\omega} \times \vec{r} + \vec{\alpha} \times \vec{r} + \vec{a} = -\nabla P' + \nabla \cdot \left(\mu_{eff} \nabla \vec{V}_r\right)^T + S_{Mp} \tag{2}$$

$$P' = P + \frac{2}{3}\rho_p k + \frac{2}{3}\mu_{eff}\nabla \cdot \vec{V} \quad (3)$$

Table 4. Solver control and some parameters used in the ANSYS CFX numerical analysis

Basic settings	• Advection scheme set to high resolution option • Turbulence numeric set to high resolution option • Convergence control set to 500 as maximum iterations. After execution of the maximum number of iterations, the domain flux imbalances are checked from the simulation report. If the domain flux imbalances are less than 0.2%, then the solution is accepted as converged. • Convergence criteria type of root-mean square of and residual target is $1e^{-4}$ for all the fluxes (mass, momentum and turbulence)
Advanced settings	• Global dynamic model control with turbulence control • Body forces control by averaging type of volume-weighted • Velocity-pressure coupling according to the Rhie-Chow option of 4^{th} power • Choose volume fraction coupling option for multiphase control • Choose pressure-based solver
Fluid pairs	• The air/water fluid is used as the fluid pair with air and water being the primary and secondary fluid respectively. • The air/water surface tension coefficient is taken as equal to $0.07199 Nm^{-1}$ at 25^0C [23] • Surface tension model with continuum surface force with air as the primary fluid • Volume fraction smoothing type of the volume-weighted • No inter-phase mass transfer
Domain initialization	• The initial Cartesian velocity in all the three flow domains is: $u = 0; v = 0; w = 0$. • The initial static pressure in all the flow domains is zero relative pressure (zero gauge pressure). • The initial turbulence in all the three flow domains is taken to be of low intensity (1%). • In all the flow domains, the initial volume fraction for air is 1 and for water is 0.

Table 5. Meaning of the symbols used in the modified RANS equations

Symbol	Meaning (or representation)
t (s)	time
α_p (-)	Volume fraction for the particular phase p
ρ_p (kg/m^3)	Density for the particular phase p
S_p (kg/s)	Continuity equation source term for the particular phase
S_{Mp} (N/m^3)	Momentum equation source term for the particular phase
$\vec{V}_r$ (m/s)	Linear equivalent of rotational velocity
∇ (-)	Del operator
$\otimes$ (-)	Dyadic symbol
μ_{eff} (kg/m.s)	Effective viscosity
$\vec{\alpha}$ (m/s^2)	Angular acceleration
$\vec{a}$ (m/s^2)	Linear acceleration
$\vec{\omega}$ (rad/s)	Angular velocity
P (N/m^2)	Pressure
P' (N/m^2)	Modified pressure
k (J/kg)	Turbulent kinetic energy

Equation (1) is the continuity equation for the two-phase flow. Equation (2) is the modified momentum equation. In both equations, the subscript 'p' refers to property of each phase. In the modified momentum equation, the expression $2\vec{\omega} \times \vec{V_r}$ is the Coriolis acceleration, $\vec{\omega} \times \vec{\omega} \times \vec{r}$ is the centripetal acceleration, $\vec{\alpha} \times \vec{r}$ is the acceleration due to unsteady change in rotational speed of the runner and $\vec{a}$ is the acceleration due to unsteady change of linear relative speed, V_r. The effective viscosity used in the momentum equation is given by equation (4). The effective viscosity is obtained by applying the eddy viscosity concept.

$$\mu_{eff} = \mu + \mu_t \tag{4}$$

where μ (kg/m.s) is the mean viscosity and μ_t (kg/m.s) is the turbulent viscosity.
The turbulent viscosity is evaluated depending on the type of the turbulent model employed in the simulation. This numerical scheme has employed the $k-\varepsilon$ turbulence model for generating initial solution that is used as initial condition for the subsequent numerical analysis using the $k-\omega$ model. These two turbulence models are widely used in industrial applications despite having some technical differences between them. The $k-\varepsilon$ model, the turbulent viscosity, given by equation (5), is linked to the turbulent kinetic energy (k) and turbulent dissipation (ε). On the other hand, for the $k-\omega$ model, the turbulent viscosity is calculated from turbulent kinetic energy and turbulent frequency (equation 6).

$$\mu_t = C_\mu \rho \frac{k^2}{\varepsilon} \tag{5}$$

$$\mu_t = \rho \frac{k}{\omega} \tag{6}$$

where C_μ (-) is a constant, ρ (kg/m^3) is the density of the fluid, k (J/kg) is the turbulent kinetic energy, ε (m^2/s^3) is the turbulent dissipation rate and ω (s^{-1}) is the mean turbulent frequency. The values of k, ε and ω are calculated from the differential transport equations for the turbulence kinetic energy and turbulence dissipation rate. The $k-\varepsilon$ model is popular for industrial applications because of its good convergence rate and relatively low memory requirements [24, 25]. It performs well for external flow problems around complex geometries. However, the model does not accurately compute flow fields that exhibit adverse pressure gradients, flow with strong curvature and jet flow.
The $k-\omega$ has relatively large memory requirements compared to $k-\varepsilon$, however, it has difficulties in converging and is sensitive to the solution initial guess [24]. The model is useful in many cases where the $k-\varepsilon$ model is not accurate, such as flows that exhibit strong curvature, separated flows and jets. In such flow phenomena, the $k-\varepsilon$ model is often recommended to be used for the initial condition for solving the $k-\omega$ model. This is the procedure that was used in the numerical analysis in this numerical study, as stated earlier.
For the volume fraction treatment of multiphase flow, due to the coexistence assumption of the free surface homogeneous multiphase flow, the effective fluid properties in each of the control volume is given in equation (7) for density and equation (8) for viscosity.

$$\rho = \sum_{p=w,a} \alpha_p \rho_p \tag{7}$$

$$\mu = \sum_{p=w,a} \alpha_p \mu_p \tag{8}$$

where α (-) is the volume fraction, subscript p is the phase (water w, or air a), ρ (kg/m^3) and μ (kg/m.s) are the density and viscosity of the averaged mixture that are used in the RANS modified equations. The air density ρ_a (kg/m$^{3)}$ is assumed to be a function of the pressure P (N/m^2) in the equation of state, equation (9).

$$\rho_a = \rho_{a,0} e^{\gamma (P - P_0)} \tag{9}$$

where the sub-index *0* marks the reference state values and γ (-) is the air compressibility coefficient.

For continuity, in each control volume, the sum of volume fraction must be equal to 1, as given by equation (10).

$$\sum_{p=w,a} \alpha_p = 1 \quad (10)$$

The volume fraction gives the proportion of the control volume that is occupied by the secondary fluid, which is water in this project. In the two phase flow problem, the secondary fluid is chosen as that which has the largest density.

5.2 Mesh properties

For numerical solutions, it is important to make sure that the mesh is of good quality so as to produce results that make sense with respect to the nature of the physical process. Also, a good quality mesh reduces computational costs. Table 6 lists mesh properties used in this study. Table 7 shows the geometric qualities of the mesh with reference to the acceptable values that are suggested in the ANSYS CFX Best Practices Guide for Turbomachinery of 2009 [24].

Table 6. Mesh properties used in the ANSYS CFX simulation study

Mesh property	Value/Action
Sizing	
Use advanced size function	On Curvature
Relevance Centre	Medium
Initial size seed	Active assembly
Smoothing	Medium
Transition	Slow
Span angle centre	Fine
-curvature normal angle	Default (18^0)
-min size	$3.5e^{-5}$m
-max face size	$3.5e^{-3}$ m
-maximum size	$0.75e^{-2}$ m
-growth rate	Default (1.2%)
Minimum edge length	$4.314e^{-3}$ m
Inflation	
Use Automatic Inflation	Program controlled
Inflation Option	Smooth transition
-Transition ratio	0.77
-maximum layers	3
-growth rate	Default (1.2%)
Inflation Algorithm	Pre
Patch conforming options	
Triangle surface mesher	Program controlled
Advanced	
Shape checking	CFD
Element mid-side nodes	Dropped
Mesh morphing	Enabled
Rigid body behaviour	Dimensionally reduced
Extra retries for assembly	Yes
Defeaturing	
Pinch tolerance	Default ($6.75e^{-5}$)m
Generate pinch on refresh	No
Automatic mesh defeaturing	On
Defeaturing tolerance	Default ($3.75e^{-5}$m)

Table 7. Mesh geometrical quality parameters at best efficiency point

Domain name	Orthogonal angle (acceptable > 20^0)	Expansion factor (acceptable < 20)	Aspect ratio (acceptable < 100)
Non-rotating zone	37.5	11	6
Rotating zone	20.3	19	22
Turbine casing	21.6	9	24
Global	21.9	19	24

As can be seen from Table 7, the mesh used in this project has favourable characteristics. The average values on orthogonality for the rotating zone and turbine casing is almost on the lowest acceptable values, possibly due to the presence of runner blades (walls) in the rotating zone. The CFX solver calculates the stated important measures of mesh quality (orthogonal angle, expansion factor and aspect ratio) at the start of a simulation run and updates them each time the mesh is deformed.

5.3 Mesh sensitivity analysis and simulations

After obtaining a good quality mesh, it is important to perform a mesh sensitivity analysis to make sure that the solution is mesh independent, as it has already been stated. The sensitivity analysis involves identifying a physical output variable to be monitored and recording its value with respect to changes in the number of mesh elements. Then the rate of change in value of the monitored variable with respect to the number of mesh elements can be evaluated from the plotted graph.

Outlet velocity from the turbine was the monitored variable for the sensitivity analysis. After convergence of the solution, the value of the outlet velocity from the monitored graph (Figure 7) was recorded together with the number of mesh elements (which were changed by varying the size of the mesh in ANSYS Meshing sub-program). Ten simulations with different number of mesh elements were performed. Then, outlet velocity was plotted against number of mesh elements (Figure 8). It can be seen from Figure 8 that after 600 x10^3 number of mesh elements, the outlet velocity was observed to be constant (at 3 m/s) with respect to increase in number of elements.

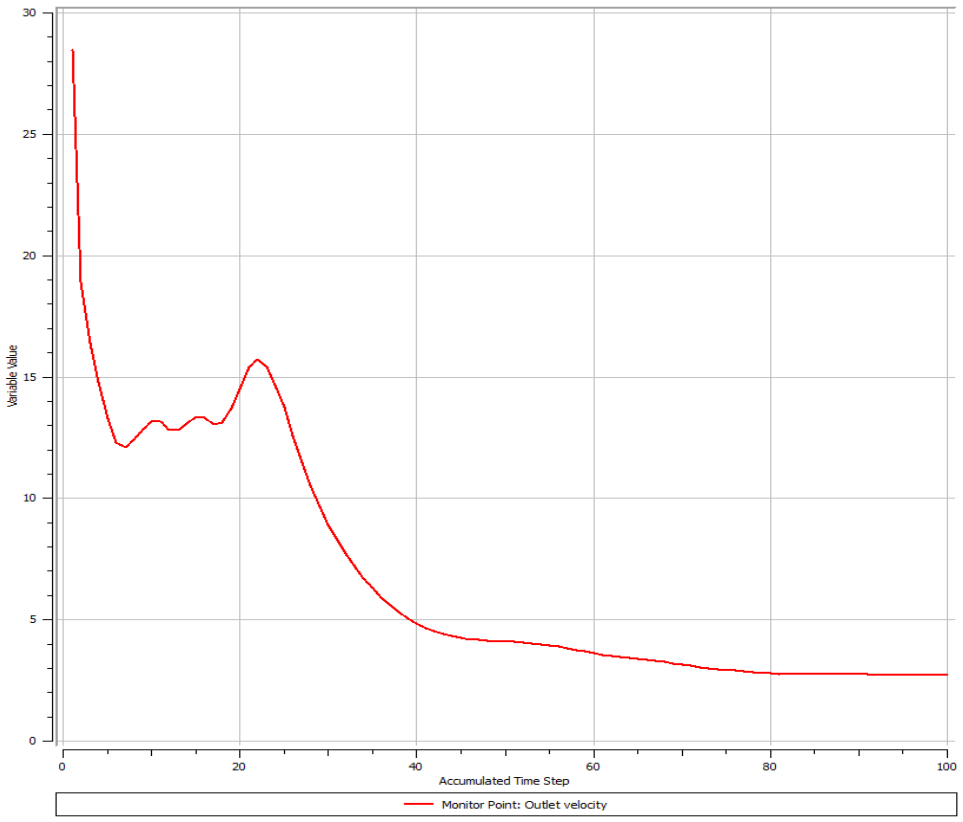

Figure 7. Graph of monitored outlet velocity during simulation against number of iterations

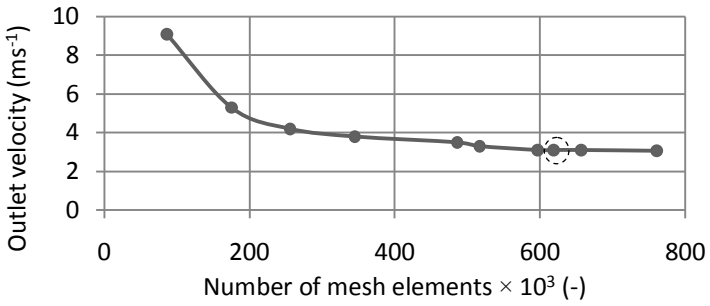

Figure 8. Graph of outlet velocity against number of mesh elements

The number of mesh elements for the final numerical analysis reported in this study was 618695 which according to the sensitivity analysis (Figure 8), is a good number of mesh for the simulation. Large number of mesh elements would cause a delay in the convergence of the solution. Table 8 shows mesh statistics for the three computational zones.

Table 8. Mesh statistics for the three flow computational zones

Computational zone	Mesh statistics	
	Nodes	Elements
Turbine Casing	133 544	492 668
Rotating	22 758	71 320
Non-rotating	14 696	54 687
Total	170 998	618 695

With respect to the first specific objective, the pressure and velocity distribution simulations were performed at best efficiency point and results processed in the ANSYS CFX-Post. The simulations at out of best efficiency points were achieved by changing the rotational speeds of the runner at constant head and valve opening. In the ANSYS CFX-Pre, the runner rotational speed was entered as the rotational speed for the 'rotating zone' (Figure 6b), while the velocity of the runner walls (representing blades) was given a relative velocity of zero.

During each simulation session, the pressure and velocity distributions were processed in ANSYS CFX – Post by creating a mid-plane across the flow domain (turbine geometry) representing the average flow plane. Apart from determining the flow pattern, the efficiency of the turbine at each simulation session was numerically determined. This was to analyze the effect of flow pattern on efficiency and to compare with the experimentally obtained values. The efficiency in the numerical analysis was calculated according to the Euler's turbine equation for the Crossflow turbine; equation (11).

$$\eta_h = \frac{1}{gH}\{(u_1 V_{u1} - u_2 V_{u2}) - (u_3 V_{u3} - u_4 V_{u4})\} \quad (11)$$

where u (m/s) and V_u (m/s) is the runner and flow peripheral speeds respectively. Subscript 1 and 2 refers to the inlet and outlet of first stage respectively; subscript 3 and 4 refers to the inlet and outlet of second stage respectively. g (m/s^2) is the acceleration due to gravity and H (m) is the effective head at the entry to the turbine. In ANSYS CFX-Post, the velocities were obtained through creating circular locations at outer diameter and inner diameter of the runner where the resultant efficiency was computed through integration.

6. Results and discussions

Flow profile at best efficiency point, in terms of velocity contours reveal that the flow in the runner does not strike the shaft, as shown in Figure 9a. Actual turbine flow picture (Figure 9b) taken using a high speed camera (Photron FASTCAM SA5) shows flow profile that is consistent with the numerically generated flow profile. Therefore the flow profile depicted in the picture validates the numerically generated flow profile. It was not possible to take a picture for the full part of the flow in the second stage due to mechanical challenges associated with positioning the camera for this purpose. The flow

past the second stage was observed using stroboscope and the flow pattern in the second stage also mimics the numerically generated pattern.

Turbine losses are at minimum level at best efficiency point. In this numerically generated flow profile, validated with actual pictures, it has been observed that at best efficiency point, the jet does not strike the shaft. Therefore, avoidance of jet from striking the shaft is important in the design high efficient CFT. The flow pattern at best efficiency point supports the theory proposed by Prof. Banki [1] that at the best efficiency point, a clear identifiable jet exists. However, this observation is in disagreement with findings from other investigators. For example, using photographic method, Durgin and Fay in 1984 [4] found out that inside the CFT runner, a free standing jet does not exist.

From Figure 9(a), it can be seen that the flow in the nozzle outlet has relatively high velocity compared to the first stage. This is due to transfer of kinetic energy from the jet to the runner. It can also be seen from the contours of the velocity field that velocity is relatively high in the second stage than in the first stage. This implies acceleration of jet and that the first stage acts as a nozzle. This is a required flow pattern for CFT design because back pressure is prevented.

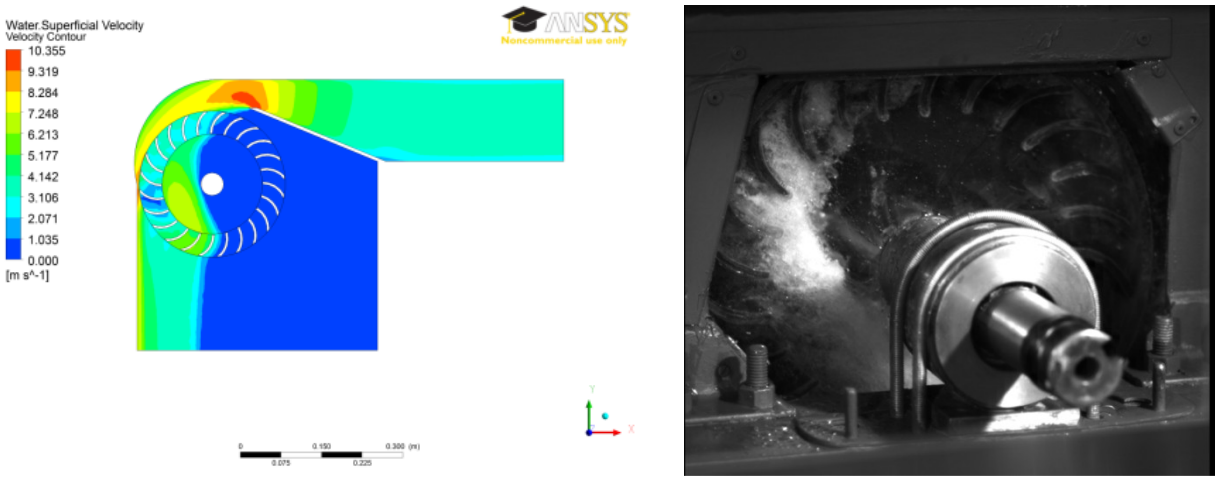

(a) (b)

Figure 9. (a) Velocity flow profile at best efficiency point using an ANSYS CFX; (b) Picture of flow profile using a high speed camera

The vector plot in Figure 10 gives a further qualitative description of the flow pattern at best efficiency point. It can be seen that the demarcation between first and second stage is short and the jet in the first stage cuts several runner blades. In the first stage, the jet covers more blades than the second stage. Therefore a considerable portion of the runner is utilized for energy transfer. This flow profile is unlike that observed in typical impulse turbine runners such as Pelton and Turgo turbines where relatively small portion of the runner is used for energy transfer.

It can also be seen from Figure 10, that at the outlet of both stages, the velocity vectors cross each other. This flow pattern supports the hypothesis that the jet leaves the stages (within blade spacing) with different flow directions resulting in flow streamlines crossing and colliding against each other. Flow pattern where the streamlines cross each other is poor for energy transfer process. It creates localized vorticities and foam in the runner that reduce efficiency.

The pressure contour diagram in Figure 11 shows that at best efficiency point, the first stage has positive gauge pressure indicating that it is operating with a degree of reaction. This is in agreement with experimental observation that at large nozzle openings, the CFT operates with a degree of reaction. It can also be seen that locations of negative pressure are identified in the runner, especially at the demarcation between stages and in the second stage. Flow pattern with pockets of negative pressure is associated with cavitation.

The flow velocity profiles for runner speeds away from the best efficiency speed (350 rpm) display some flow patterns worth noting.

It can be seen from the velocity contours (Figure 12) that as the runner speed increases, the jet in the runner drifts way from the shaft. The change in absolute velocity vector of the jet at first stage outlet as a result of change in runner periphery velocity may explain the drifting away of the jet from the shaft. The

absolute velocity is the vector sum of relative velocity and runner periphery velocity. It can also be seen that the demarcation between the two stages progressively becomes small as the runner speed increases.
The velocity contour diagrams also reveal that as the runner speed increases beyond the best efficiency point, at high speeds, there is back flow. This implies that at these speeds, the CFT is operating with a pumping effect. This can be seen with speeds of 500 rpm and 600 rpm velocity contour diagrams and the 600 rpm velocity vector diagram. The flow with back pressure is due to the increased contribution of the centrifugal forces on the flow as the runner speed increases.
Referring to velocity contour and vector at 100 rpm in Figures 13(a) and 14(a) respectively, it can be seen that at lower runner speeds, the flow in the runner strikes the shaft, resulting in increased incidence losses. Figure 14(b) shows the actual picture of the flow in the runner taken at 100 rpm. It can be seen that the jet strikes the shaft and the actual flow pattern mimics the numerically generated flow profile.
Numerical flow analysis results when the CFT operates outside the best efficiency point are presented in Figure 12.
The flow pattern with back pressure reduces the resultant flow that passes through the runner to generate power. Also, back pressure reduces the amount of pressure energy that could be imparted to the runner due to reaction effect. This numerical observation is in agreement with the results obtained by Varga in 1959 [26]. He experimentally found out that the increased speed of the modified CFT runner affects the flow through the runner. However, this is a deviation from the operation of a typical impulse turbine as originally proposed by Prof. Banki.
In Figure 15, the pressure contours when the CFT operates away from the best efficiency point do not show significant differences. At all operating speeds, the jet enters the first stage with positive gauge pressure. It can be seen that the static pressure in the nozzle entry arc increases with runner rotational speed. The increase in static pressure at constant head indicates presence of back pressure. Again, this pressure profile does not support the operating principle of a pure impulse turbine.

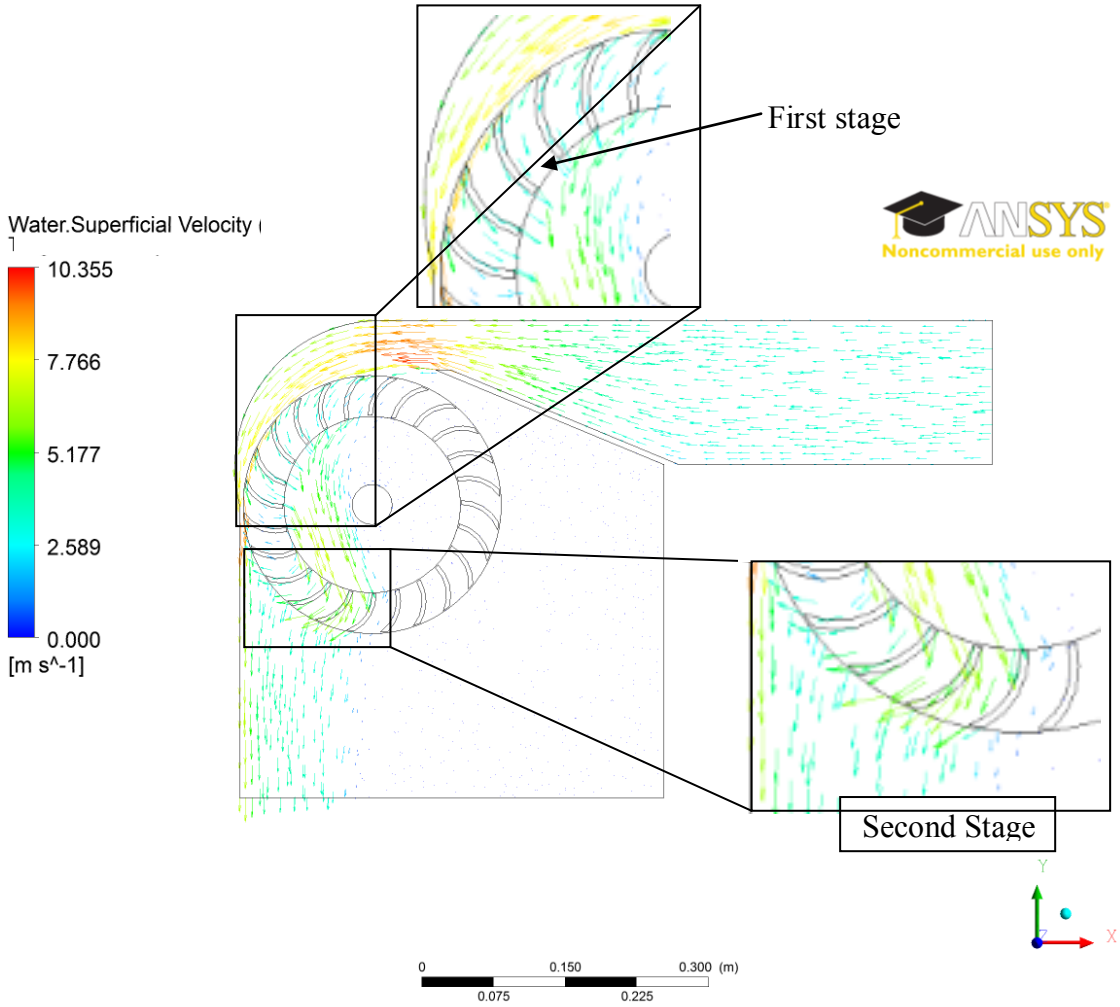

Figure 10. Vector plot of flow in the Crossflow turbine at best efficiency point

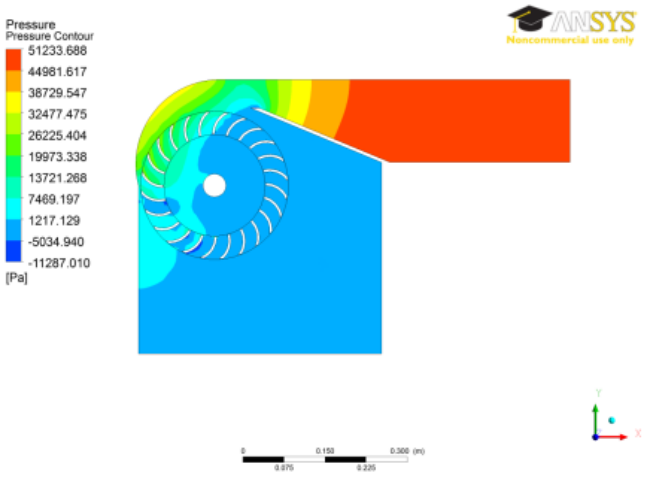

Figure 11. Pressure contour at best efficiency point

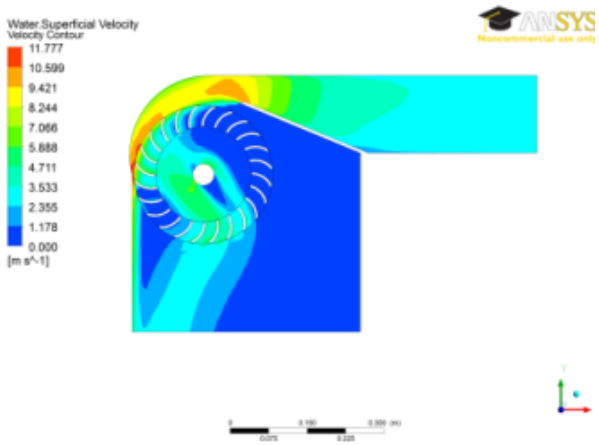

100 rpm

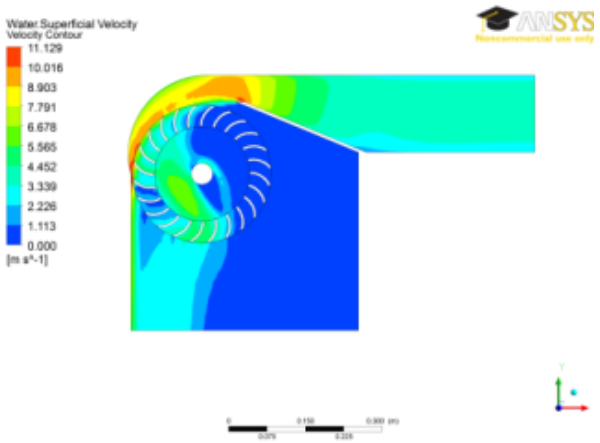

200rpm

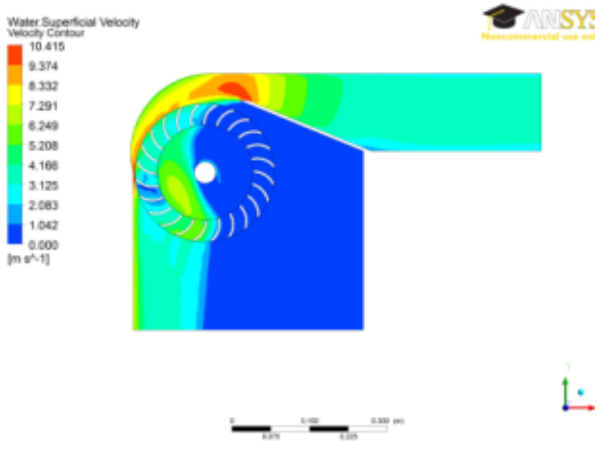

300rpm

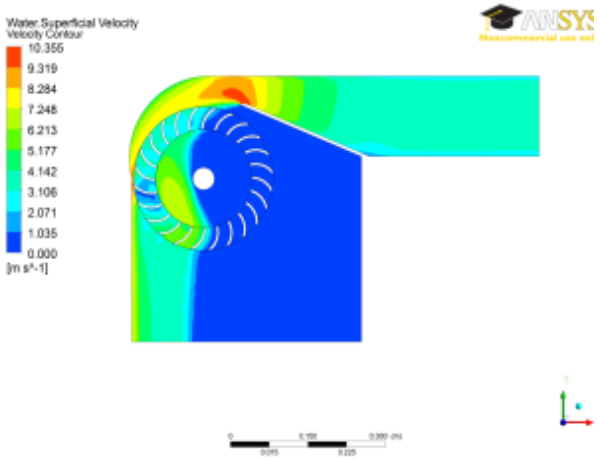

350rpm

Figure 12. (Continued)

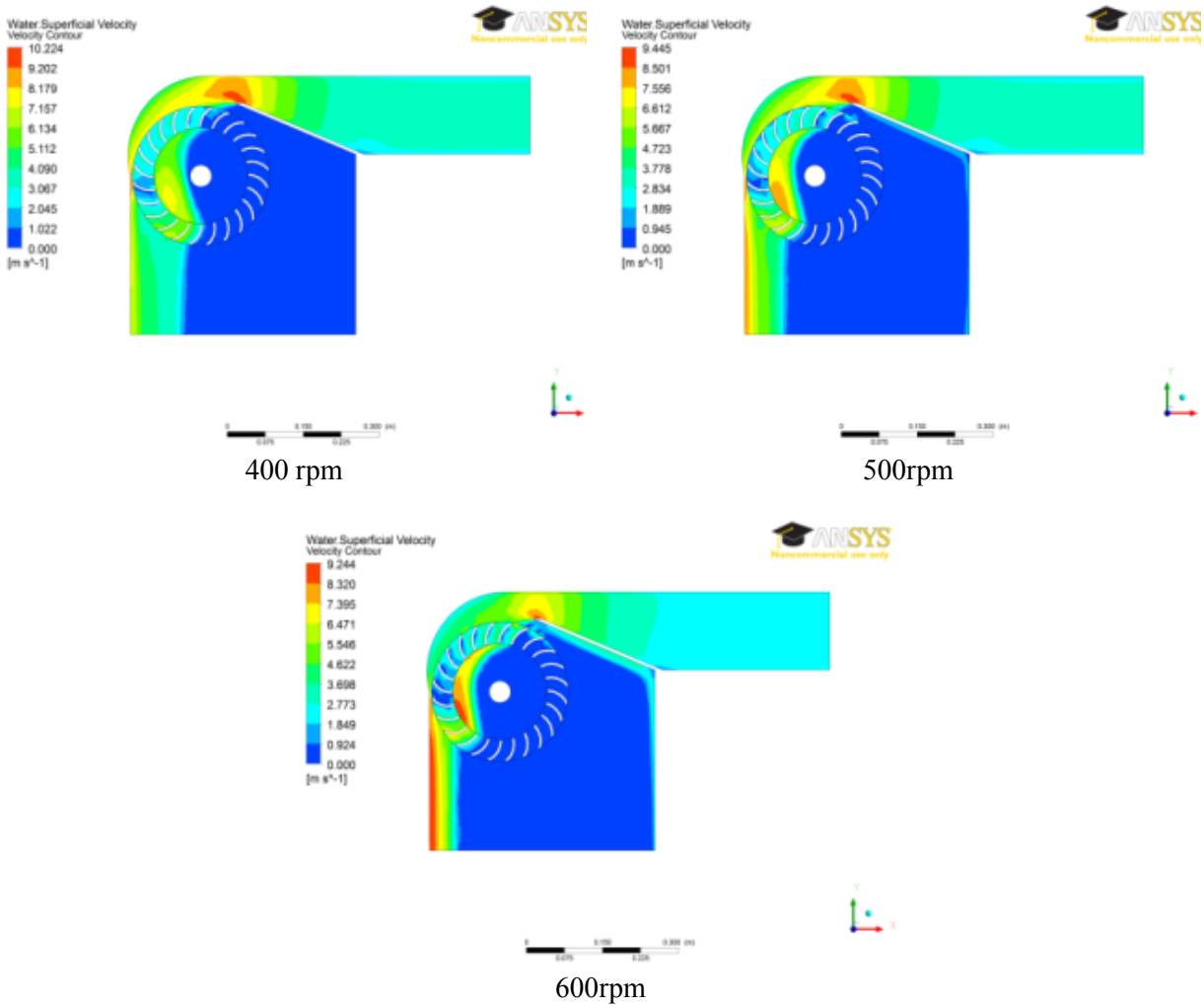

Figure 12. velocity contours for various runner speeds away from best efficiency point

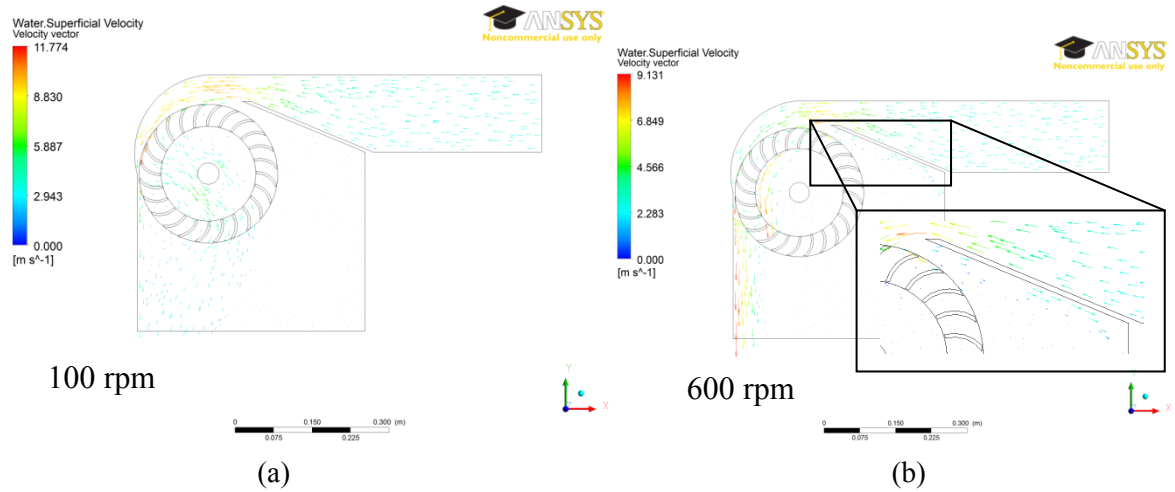

Figure 13. (a) Velocity vector diagram at 100 rpm runner speed; (b) Velocity vector diagram at 600 rpm runner speed

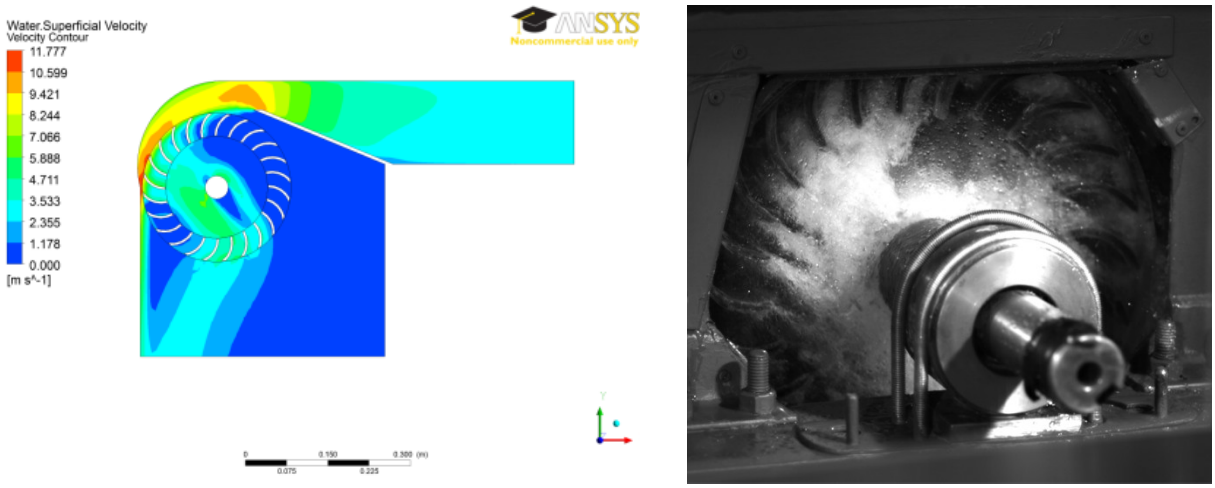

(a) (b)

Figure 14. (a) The velocity contour at 100rpm; (b) picture of flow in the runner at 100 rpm

The hydraulic efficiency was numerically evaluated from equation (11) and compared with the turbine efficiency that was measured experimentally on the same CFT model in 2013 at Waterpower Laboratory of the Norwegian University of Science and Technology. This was to evaluate the extent to which the numerical analysis predicts the actual turbine performance. The tests in Figure 16 were performed at 5m head and valve opening of 80%.

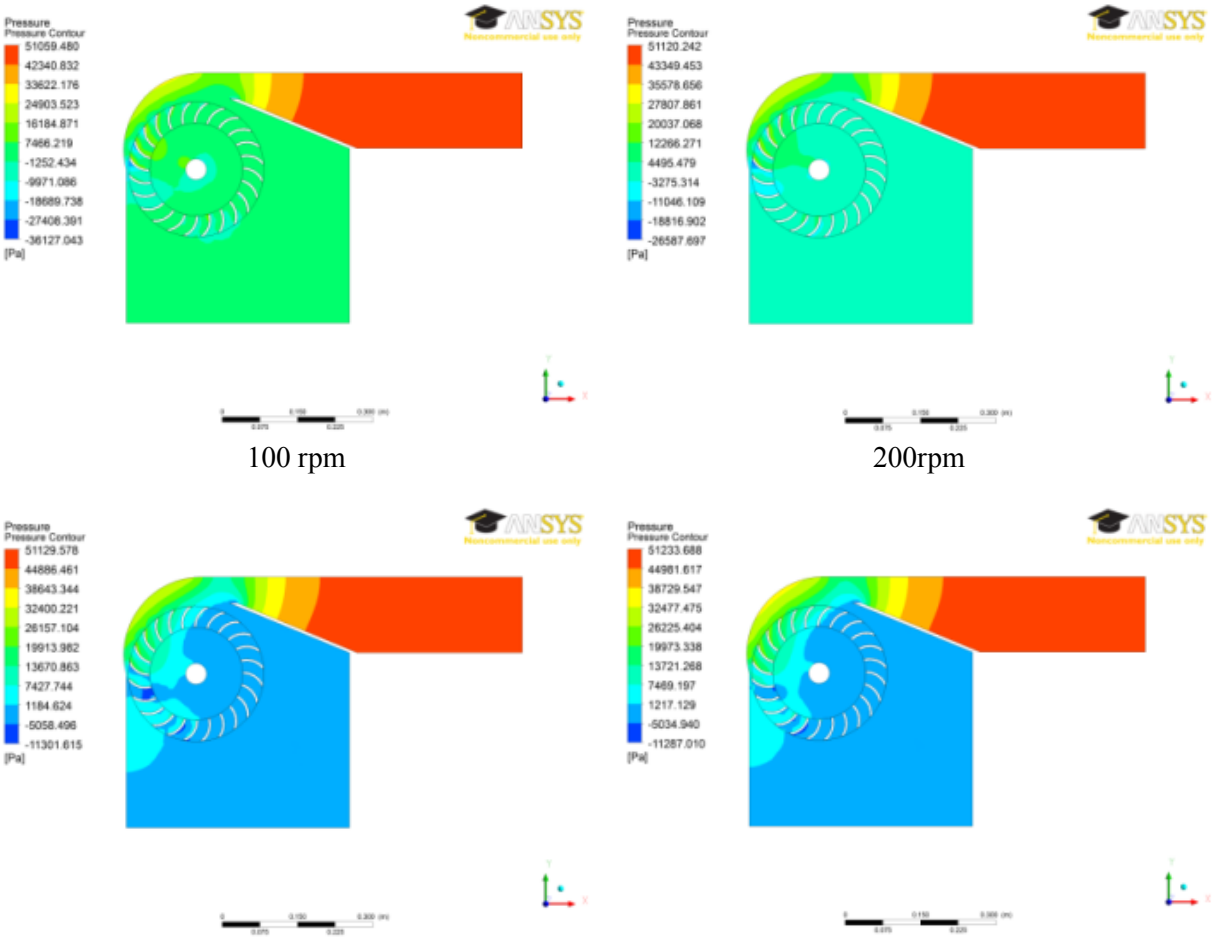

100 rpm 200rpm

300rpm 350rpm

Figure 15. (Continued)

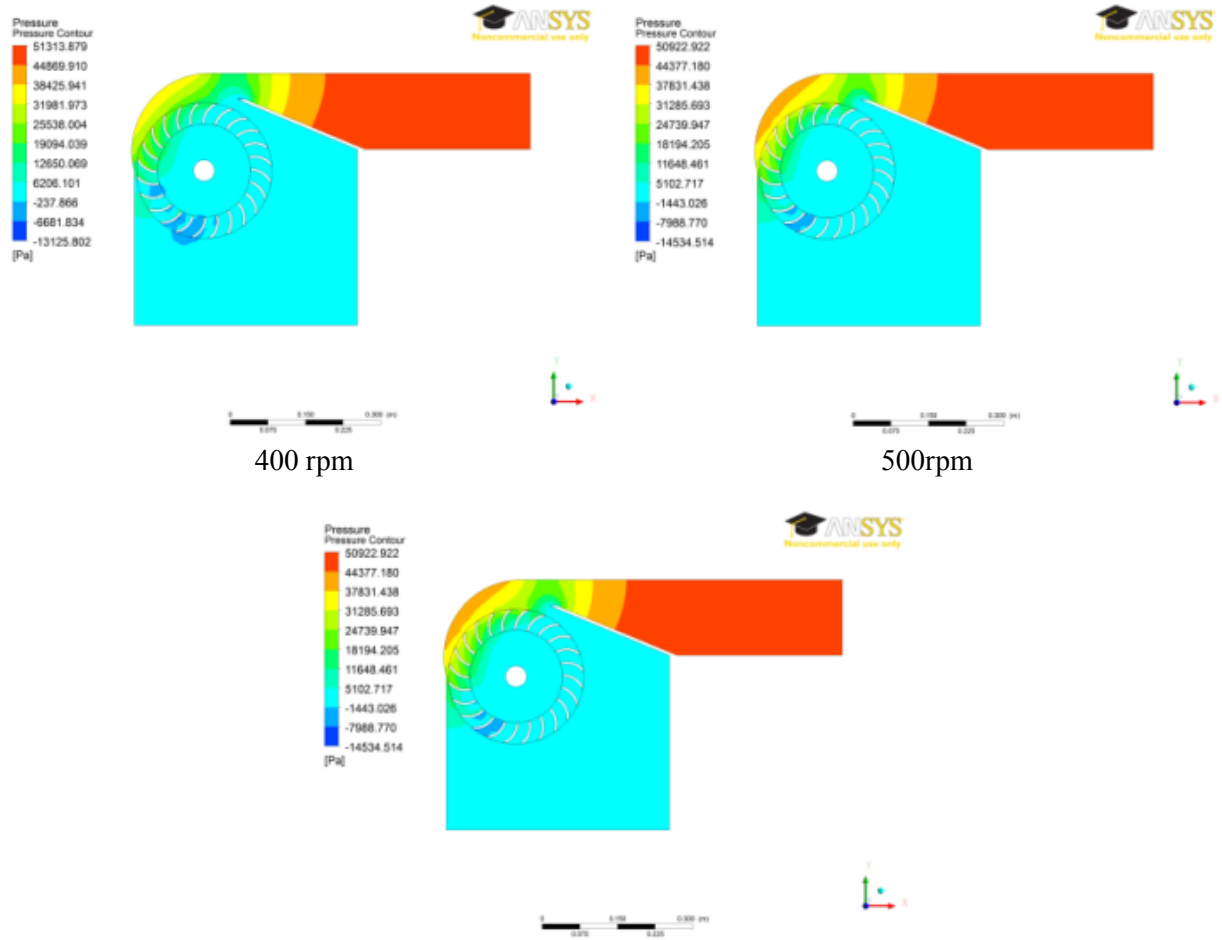

Figure 15. Pressure contours for various runner speeds away from the best efficiency point

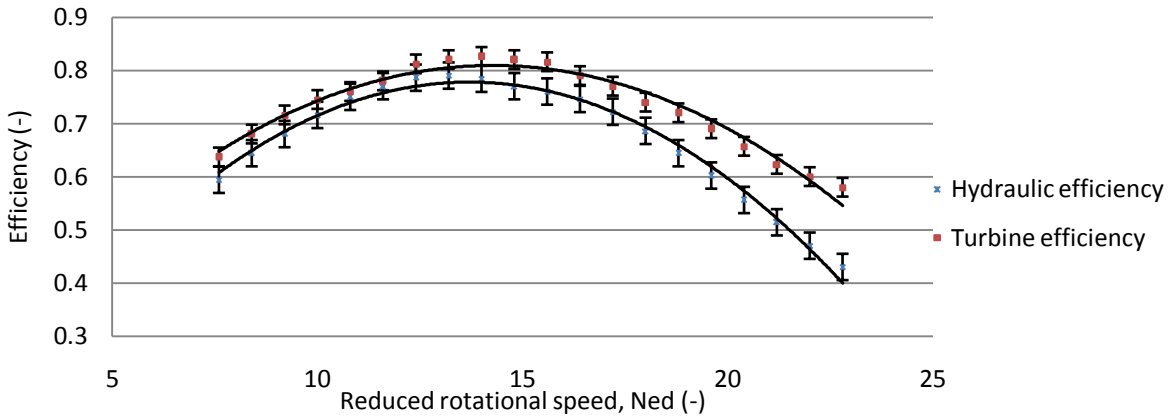

Figure 16. Variation of hydraulic efficiency and turbine efficiency with runner rotational speed.

It can be seen from Figure 16 that the graphs for experimental turbine efficiency and numerically determined hydraulic efficiency show similar trends. As expected from Euler's turbine equation, the relationship between the efficiency and rotational speed is quadratic for both graphs. The quadratic relationship with maximum values corresponding to the maximum efficiency speed can be seen from both graphs. The maximum efficiency values corresponding to reduced speed of around 13 are observed. The standard error bars on the experimental results are included. In both graphs, the trend lines are mostly within the standard error bars of the data points.

Despite the consistency, the numerically determined hydraulic efficiency tends to give higher values especially for runner speeds exceeding best efficiency point, thus indicating that numerical analysis over-predicts the performance. One of possible the reasons for over-prediction of efficiency is that the mechanical efficiency of the turbine is not considered in the numerical calculations. The mechanical efficiency increases with runner speed. Hence at higher speeds, the contribution of mechanical losses is increased which lowers the shaftpower and widens the difference between the efficiencies.
It is inevitable for the discrepancies (both qualitative and quantitative) in numerical and experimental analyses to be present due to several reasons. Numerical analyses are associated with numerical errors and it is difficult to describe mathematically some flow processes. Numerical errors arise from the numerical procedure, mesh, data processing and geometric complexity of the turbine. Further, assumptions on the boundary conditions and turbulence model are major sources of numerical errors and may generate unrealistic simulation results.
In this numerical study, the numerical approach in the ANSYS CFX homogeneous free surface model does not support buoyancy and Coanda effect. Therefore, segregation between phases that occurs due to the gravitational action on the flow has not been modelled. Further, the deflection of the jet due to Coanda effect has not been modelled. However, due to complex nature of the flow and geometry of flow domain, numerical approach has proven to be superior in the design of 'partial' turbines such as the Crossflow.

7. Conclusions and recommendations

The conclusions that can be drawn from this numerical study of the flow profile and performance of Crossflow turbine are as follows:

1. The numerically determined performance results compare favorably with the experimental results. This shows that the CFD is an important tool for the design of 'partial' turbines such as the Crossflow.
2. The study shows that Crossflow turbine, at best efficiency point, operates using both impulse and reaction principles.
3. Incidence losses are greatly reduced when the jet does not strike the shaft in the runner. This shows that avoidance of jet from striking the shaft is important in the design of a high efficient Crossflow turbine.
4. Some pockets of negative pressures were identified in the flow in the runner. This signals the turbine runner being susceptible to cavitation; a problem which has been identified in practice.
5. At constant head and valve opening, the flow pattern in the runner depends on runner speed. At lower speeds, the flow in the runner strikes the shaft leading to increased incidence losses. At higher speeds, back flow in the runner was observed, again reducing the efficiency of the turbine.

On improving the efficiency over a range of operational runner speeds, it is recommended to consider designing the Crossflow turbine that does not have the shaft inside of the runner where crossed-flow jet passes through. Since the shaft provides an additional structural integrity to the turbine runner (together with the blades that are welded to the discs), it is important to carry out another numerical study, using finite element analysis, to investigate the effect of removing the shaft on performance and structural strength of the runner.

Acknowledgement

The authors appreciate the support from NORAD under the Energy and Petroleum (EnPe) Program for funding this research at Waterpower Laboratory, Department of Energy and Process Engineering, Norwegian University of Science and Technology.

References

[1] Mockmore C, Merryfield F. The Banki water-turbine. Engineering Bulletin, Series Number 25, Oregon State University, Corvallis, United States of America, 1949.
[2] Nakase Y, Fukutomi J, Watanabe T. A study of the Crossflow turbine, effects of nozzle shape on its performance. Journal of small hydropower fluid machinery, American Society of Mechanical Engineers (ASME), 1982, pp: 29-133.
[3] Johnson W, Ely R, White F. Design and test of an inexpensive Crossflow turbine. In Proceedings of American Society of Mechanical Engineers (ASME) annual symposium on small hydropower fluid machinery, New York, USA, 1982.

[4] Durgin W, Fay W. Some fluid flow characteristics of a Crossflow type hydraulic turbine. In Proceedings of American Society of Mechanical Engineers (ASME), Winter Annual Meeting on small hydropower fluid machinery, New Orleans, USA, 1984.
[5] Khosrowpanah S. Experimental study of the Crossflow turbine. PhD dissertation, Colorado State University, USA, 1984.
[6] Hothersall R.J. A review of the Crossflow turbine. In Proceedings of American Society of Civil Engineers (ASCE) on Waterpower, New York, N.Y., 1985, vol. 2, page 914.
[7] Ott R, Chappel J. Design and efficiency testing of a Crossflow turbine. In Proceedings of American Society of Civil Engineers (ASCE) on Waterpower, New York, N.Y., 1989, 1534-1539.
[8] Desai V, Aziz N. Parametric evaluation of Crossflow turbine performance. Journal of Energy Engineering, 1994, vol. 120, no. 1. pp: 17-34. American Society of Civil Engineers.
[9] Olgun H. Investigation of the performance of the Crossflow turbine. International Journal of Energy Research, issue 22, pp 953 – 964, 1998. John Wiley & Sons, Ltd.
[10] Andrade J, Curiel C, Kenyery F, Aguillon O, Vasquez A, Asuaje M. Numerical investigation of the internal flow in a Banki turbine. International Journal of Rotating Machinery, 2011, vol. 2011, article ID 841214, 12 pages.
[11] Zoppe B, Pellone C, Maitre T, Leroy P. Flow analysis inside a Pelton turbine bucket. Journal of Turbomachinery, 2006, vol. 128, issue 3, pp 500-511.doi: 10.1115/1.2184350
[12] Fukutomi J, Senoo Y, Nakase Y. A numerical method of flow through a Crossflow runner. JSME International Journal, 1991, series II, vol. 34, no. 1, pp 44-51.
[13] Fukutomi J, Nakase Y, Ichimiya M, Ebisu H. Unsteady fluid forces on a blade in a Crossflow turbine. JSME International Journal, 1995, series II, vol. 38, no. 3, pp 404-410.
[14] Pereira N.H, Borges J.E. Study of the nozzle flow in a Crossflow turbine. International Journal of Mechanical Sciences, 1996, vol 38, n. 3, pp 283-302.
[15] Arzola F, Rodriquez C, Martin J, De Andrade J, Vasquez A, Asuaje M. Technical assessment for overhaul project in small hydropower plant. In Proceedings of the 24th Symposium on hydraulic machinery and systems, Iguassu, Brazil, October 2008.
[16] Choi Y, Lim J, Kim Y, Lee Y. Performance and internal flow characteristics of a Crossflow hydro turbine by the shapes of nozzle and runner blades. Journal of Fluid Science and Technology, 2008, vol.3, no. 3, pp. 398 – 409.
[17] Khosrowpanah S, Fiuzat A, Albertson M. Experimental study of Crossflow turbine. Journal of Hydraulic Engineering, 1988, vol. 114, no. 3 pp: 299-314. American Society of Civil Engineers (ASCE).
[18] JLA & Co. Limited. Crossflow turbine Information. Product information by the JLA & Co, a turbine manufacturing company in B-4520 Moha, Belgium, 2010. Available online at <http://www.jlahydro.be/en/jla-cross-flow-turbines> [12 July 2013].
[19] Ossberger Limited. Ossberger turbine information. Ossberger Limited, Weissenburg/Bavaria Germany, 2013. Available <http://www.ossberger.de/cms/pt/hydro/ossberger-turbine/> [20 August 2013]
[20] Joshi B, Seshadri V, Singh S. Parametric study on performance of Crossflow turbine. Journal of Energy Engineering, 1995, vol.121, no. 1, pp: 28-45. American Society of Civil Engineer (ASCE).
[21] Haimerl L. A. The Crossflow turbine. In Conference proceedings on Water Power, London (UK), 1960, vol. 12 pp: 5-23.
[22] ANSYS. ANSYS CFX Solver Modelling Guide. Published by the ANSYS, Inc. in United States of America, 2010, Release 13.
[23] Vargaftik, N. B.; Volkov, B. N.; Voljak, L. D. J., 1983. International tables of the surface tension of water. Journal of Physical and Chemical Reference Data, vol.12, No. 3, pp: 817-820. Published by American Institute of Physics (AIP) Publishing.
[24] ANSYS CFX, 2009. Best Practices Guide for Turbomachinery. ANSYS CFX – 12 Reference guide. Published by the ANSYS, Inc. in United States of America, 2009, Release 12.
[25] Rodi W. Turbulence models and their application in hydraulics: A state of the art review. Taylor and Francis, 1993, Third Edition, ISBN 9789054101505.
[26] Varga J. Tests with the Banki water turbine. Journal of the Hungarian Academy of Sciences, 1959, vol. pp: 779-102.

Chiyembekezo S. Kaunda is an energy lecturer and an energy consultant. He is an academic member of staff at the University of Malawi but currently pursuing a sandwiched Ph.D in microhydro systems at University of Dar es Salaam and Norway University of Science and Technology. He has an MSc in Thermofluids and Energy Systems obtained from Kwame Nkrumah University of Science and Technology, Kumasi, Ghana in 2006. Has five publications in the area of small-scale hydropower systems. He has reviewed several Government of Malawi documents on energy and environment as well as UNIDO World Small Hydropower Development Report (2013). Has conducted consultancies in energy project evaluation and climate change mitigation in Malawi. He has attended training workshops in hydropower and environment, energy and development, rural electrification and climate change. Mr. Kaunda's main research interests are in renewable energy, environment and climate change.
E-mail address: kaundas@gmail.com or skaunda@poly.ac.mw

Cuthbert Z. Kimambo is an Associate Professor of renewable energy at University of Dar es Salaam, Tanzania. He has an MSc and Ph.D in Mechanical Engineering from Reading University and London City University, United Kingdom, respectively. He lectures renewable energy and supervises many MSc and Ph.D students in energy engineering. Prof. Kimambo's main research interests are in renewable energy especially solar, hydro and wind. He has several publications in renewable energy. He was once the Chairperson for the Tanzania Renewable Energy Agency.
E-mail address: kimambo@udsm.ac.tz

Torbjorn K. Nielsen a full Professor of hydropower at Norwegian University of Science and Technology (NTNU) and is in charge of the Waterpower Laboratory. He is an expert in hydropower turbine design and transient analysis. Has conducted several consultancies in these areas. He lectures and supervises several MSc and PhD students. Prof. Nielsen's main research interests include design of turbomachinery and their verification using numerical methods as well pressure transient analysis in hydropower systems.
E-mail address: torbjorn.nielsen@ntnu.no